RSC Advances

RSC Publishing

REVIEW

View Article Online
View Journal | View Issue

Elements of functional ion/block copolymer hybrids

Cite this: *RSC Adv.*, 2013, **3**, 23895

Feifei Xue* and Shichun Jiang*

Received 10th July 2013
Accepted 10th September 2013

DOI: 10.1039/c3ra43504k

www.rsc.org/advances

Block copolymers (BCPs) self-assemble into well-ordered morphologies ranging from spheres to cylinders to lamellae depending upon their chemical structures, preparation conditions and dynamic processes. Recently, ion/BCP hybrids have become highly attractive materials due to their flexibility, processability, self-assembling ability and novel features of inorganic components such as electronic, magnetic and optical properties. Therefore, to control the structure and functionalization of ion/BCP hybrids has been a significant challenge in material preparation and manufacturing. The progress of ion/BCP hybrids in bulk and thin films including the influence of ions upon the phase behavior of AB diblock and ABC triblock copolymer bulks has been reviewed, starting from fundamental principles and extending to recent promising developments, along with contributions to aligning block copolymer nanostructures and important applications such as solid-state batteries, fuel cells, nanolithography, templating, and patterning of nanoparticles.

1. Introduction

Block copolymers (BCPs) represent a subject of broad current research emphasis across the full spectrum of macromolecular chemistry and physics, ranging from the development of new synthetic strategies and molecular architectures to applications of advanced theoretical and computational methods.[1] The development of BCPs originated with the discovery of termination-free anionic polymerization, which made it possible for sequential addition of monomers to various carbanion-terminated ("living") linear polymer chains.[2] Almost fifty years after the preparation of the first laboratory samples, scientific interest in these materials continues to grow, as does the global market for BCP materials. However, the current abundant applications of BCPs are "scalar" in the sense that they do not take advantage of any particular nanostructure; rather, they are useful because they retain important features of their constituent homopolymers while suppressing macroscopic phase separation. For example, thermoplastic elastomers are important in a variety of applications such as polystyrene-*block*-polyisoprene-*block*-polystyrene (PS-*b*-PI-*b*-PS), but it is primarily the microphase separation of the styrene and isoprene segments that leads to robust and reusable elastomeric behavior, rather than any particular ordered structures.[3] In the future, new applications of block copolymers are much more likely to be "vectorial" in nature, relying not only on the properties of the components, but also on the particular doping, spatial extent, connectivity, and orientation of the nanodomains.[1]

To further explore the novel properties of block copolymers and develop more performance requirements, a new spotlight has been focused on ion/BCP hybrids, because they have high ionic conductivity, stable electrochemical characteristics, and excellent mechanical properties.[4–8] Researchers found that BCPs with an ion-dissolving block, typically polyethylene oxide (PEO), polymethyl methacrylate (PMMA) or polyvinyl pyridine (PVP), and a non-conducting block such as polystyrene (PS),[9] coordinated with ions could generate novel features in the field of morphological changes of polymer assemblies, phase behavior, or nanostructure ordering.

Zhang *et al.*[10] reported that the addition of ions in micromolar ($CaCl_2$ or HCl) or millimolar (NaCl) concentrations can change the morphology of "crew-cut" aggregates of amphiphilic block copolymers in dilute solutions. In addition to spherical, rodlike, and univesicular or lamellar aggregates, unusual large compound vesicle morphology can be obtained from a single block copolymer. Mullin *et al.*[11] found that lamellar poly(styrene)-*block*-poly(ethylene oxide) (PS-*b*-PEO) block copolymers could be coordinated by lithium bis(trifluoromethane-sulfone)imide (LiTFSI) salt. In this system, the mechanical properties are dominated by the rigid PS block, whereas the conductivity depends crucially on the connectivity of the PEO domains where the LiTFSI molecules reside. The salt diffusion coefficient increases as the molecular weight of the PEO block, M_{PEO}, increases. It is similar to previously reported trends which indicated that the ionic conductivity of block copolymer electrolytes, also increases with increasing M_{PEO} and reaches a plateau. Noro *et al.*[12] reported that block copolymer was blended with metal salt *via* metal-to-ligand coordination in a polar solvent with coordinating ability, pyridine, to obtain macroscopically homogeneous hybrid films. The morphology of the observed system can be

School of Materials Science and Engineering, Tianjin University, Tianjin 300072, China. E-mail: ffxue@tju.edu.cn; scjiang@tju.edu.cn

controlled by a stoichiometric balance between the BCP units and the metal salt. For example, in polystyrene-*block*-poly-(4-vinylpyridine) (PS-*b*-P4VP, M_n = 37k, φ_s = 0.79) BCP, the domain expansion and morphology transition could be observed as the amount of added $FeCl_3$ increased. Kim *et al.*[13] found that ion complexation within the cylinder-forming block copolymer thin films affects the ordering process of the copolymer films during solvent annealing, significantly enhancing the long-range positional order. Small amounts of alkali halide or metal salts were added to PS-*b*-PEO, on the order of a few ions per chain, where the salts coordinate with the PEO block. The orientation of the cylindrical microdomains strongly depended on the salt concentration and the ability of the ions to complex with PEO. The copolymer remained highly ordered at large degrees of swelling and demonstrated long-range positional correlations of the microdomains in the swollen state with increasing added salts, which holds promise as a route to addressable media. Some researchers found that metal-precursor salts can be confined within the nanoscopic microdomains of the block copolymers, and through subsequent reduction reactions, the precursor salts can be converted to the corresponding metal, providing a simple route for the generation of metallic nanoparticles within the minor component phase of the block copolymer.[14–17] For example, polystyrene-*block*-poly(vinylpyridine) copolymer (PS-*b*-PVP) micellar structures have been successfully used to fabricate various metal and metal–oxide nanoparticle 2-D arrays.[18]

Thus it can be seen that ion/BCP hybrids have made great progress in many areas and been the focus of a great deal of research activity in contemporary macromolecular science.[1] This review focuses on the particular facet of macromolecular science, involving both historical development and the promising potential of the topic, which mainly introduces the influence of ion upon the phase behavior of bulk BCPs and the thin film structure transitions or reorientations both on experiments and theory. Meanwhile, the relationship between the conductivity of the BCPs electrolytes and ion concentration, ion distribution, or other factors are resolved. In addition, a brief description about ion-triggered morphology transition in solutions is introduced.

2. Ion influence upon phase behavior of BCPs in bulk

2.1 Order–disorder transition (ODT)

The phase behavior of block copolymers can be described theoretically by different approaches.[19,20] According to mean-field theory, the phase behavior of diblock copolymers is dictated by the Flory–Huggins segment–segment interaction parameter, χ, the degree of polymerization, N, and the composition, φ, with the product $N\chi$ determining the degree of segregation. In the case of $N\chi < 10$, the system is ruled by entropic terms, resulting in a disordered phase. Under the condition $N\chi > 10$, enthalpic terms dominate, causing an order–disorder transition (ODT) where the different segments segregate into a variety of ordered periodic microstructures. Plenty of research groups have investigated theoretically or experimentally the phase behavior and order–disorder transition temperature (T_{ODT}) of various kinds of block copolymers. Generally, the

Table 1 Experimental methods and related theories to determine T_{ODT}

Method	Plots	Related theory
Scattering method (small angle X-ray and neutron scattering)	$1/I$ *vs.* 1/temperature	Random phase approximation
Rheological method	G' *vs.* temperature	Critical phenomena
	log G' *vs* log G''	Tube theory
Depolarized light scattering (birefringence)	Light intensity *vs.* temperature	
Differential scanning calorimetry	Heat capacity (or heat flow) *vs.* temperature	
Fourier transformed infrared spectrum	Absorbance *vs.* temperature	

T_{ODT} is controlled by the volume fraction of one component (f), the conformational asymmetry of each block, and the degree of microphase separation χN. The common experimental methods to determine the T_{ODT} of block copolymers are summarized in Table 1.[21] Among them, small angle X-ray and neutron scattering (SAXS and SANS), and rheological methods have been widely used. The scattering method can determine the exact microdomain structure but relatively expensive and large facilities providing X-ray (or neutron) sources should be used to measure the scattering intensity (I). On the other hand, the rheological method is easily accessible and rheological properties such as storage and loss moduli (G' and G'') and viscosity are measured to determine the T_{ODT} of block copolymers. However, compared with the scattering method, the microdomains in the equilibrium could not be measured because of the existence of a shearing force.

As an evidence of the formation of ionic complexes, dramatic changes in T_{ODT} of BCPs that had strong coordination interactions with the metal ions, such as PEO or PVP block, were firstly and widely observed. Adding even a small amount of salt led to an increase of the T_{ODT} by tens of degrees celsius.[22–24] This trend in the temperature change was attributed to the enhancement of the effective interaction parameter, χ_{eff}, with the formation of lithium–PEO complexes.[25,26]

For salt-free block copolymers, a single Flory–Huggins parameter χ, describes all the properties of the system in both the ordered and disordered phases. In other words, the parameter χ can be obtained either by the domain spacing in the ordered phase or by the behavior of the structure factor in the disordered phase. All properties will yield the same χ if the regression is carried out consistently.[27] And, widely accepted, the local interactions in block copolymer melts can be described by the parameter χ with a temperature dependence:

$$\chi = \frac{A}{T} + B \quad (1)$$

The parameter χ and its temperature dependence for some systems has also been experimentally obtained by small angle

X-ray scattering analysis, obtaining the expression $\chi = \chi_S + \chi_H/T$.[28] This functional form of the interaction parameter is consistent with the notion that χ may be written as the sum of an enthalpy and an entropic contribution.

For ion-containing block copolymers it is often assumed that the ions, which are dissolved in only one of the blocks, simply modify the segmental interactions such that the whole system can still be described as a binary system with a new χ_{eff}:

$$\chi_{eff}(r) = \frac{A(r)}{T} + B(r) \quad (2)$$

where r denotes the molar ratio between the ions and the monomers of ion-containing blocks. Experimentally, χ_{eff} has been identified by the changes in the structure factor of the disordered phase,[28] the shift in the phase boundaries,[29,30] and the change in the domain spacing of the ordered phases.[31,32] However, it is noteworthy that the effective parameter χ_{eff} reflects the combined effects of several contributing factors, whose relative contributions may depend on the state of the system or on the properties studied. Therefore, χ_{eff} determined from the domain spacing of the ordered phases may not coincide with that determined from the spinodal of the disordered phase using the random phase approximation. Similarly, the χ_{eff} determined from the spacing of different ordered phases may not be the same.[32] Theoretically, Wang *et al.* argued that the χ_{eff} determined from the spinodal of the disordered phase is a more fundamental measure of the effective interaction between the two blocks.[27]

The experimental results proved that χ_{eff} is affected by salt concentration, temperature, salt counterions, and chain conformation. Young *et al.* reported a linear relationship between χ_{eff} and salt concentration in PS-*b*-PEO:LiX (X = ClO_4^-, $CF_3SO_3^-$, AsF_6^-) systems, where χ_{eff} is estimated according to the strong segregation theory.[31] The neat sample and domain spacing of salt-doped samples at 166 °C were used to estimate χ_{eff}, which showed a linear relationship with salt concentration ([Li]/[EO]) for both the $LiClO_4$-doped and $LiCF_3SO_3$-doped systems (Fig. 1a). By comparing the three lithium salts, they noted that χ_{eff} related to counterions. $LiAsF_6$-doping shows the largest increase in segregation strength (χ_{eff}) at a given salt concentration, which relates to the weaker Lewis base character of AsF_6^- relative to the other lithium counterions (Fig. 1b). The influence of chain conformation on χ_{eff} was investigated by Wang *et al.* using lithium-complexed PS-*b*-PMMA copolymers by small-angle neutron scattering (SANS) as a function of temperature and the percentage of carbonyl groups coordinated with lithium ions.[28] They fitted scattering profiles accurately and got χ_{eff} with an error limit of at most 0.0001.

In general, the linear relationship between χ_{eff} and salt concentration can be concluded as

$$\chi_{eff} = \chi + mr \quad (3)$$

where χ is the intrinsic Flory–Huggins parameter for the salt-free system, r is the molar ratio between ions and the monomers, and the slope m depends on the anion type. The values of m in the cases of $LiAsF_6$, $LiClO_4$ and $LiCF_3SO_3$ in PS-*b*-PEO are 5.70, 5.53 and 3.90, respectively. Interestingly, this equation (eqn (3)) could be extended to other ion-containing BCPs systems. In the case of LiCl added polystyrene-*block*-poly(methyl methacrylate) (PS-*b*-PMMA) copolymers, χ_{eff} increases from 0.0360 to 0.0368, when r increases from 0 to 0.1, indicating that m is about 10^{-4}.[28] Wanakule *et al.* reported that m for PS-*b*-PEO/LiTFSI is 1.56.[33] Notably, m is a system dependent constant. It was also found that m decreases with increasing anion radius a,[29] and this dependence provides a means for estimating the parameter m. Wang's group[34,35] theoretically indicated that m could be calculated with independently determined parameters such as the dielectric constants of the two phases, the size of the ions, the extent of dissociation, the dielectric constant of the block copolymer microphases, and the statistical segment lengths of the copolymer chains.

The transition process from disordered to ordered phases was recently studied by SAXS and ionic conductivity measurements. For PEO-*b*-PS containing lithium LiTFSI, near the transition, the scattering intensity exhibits a superposition of both

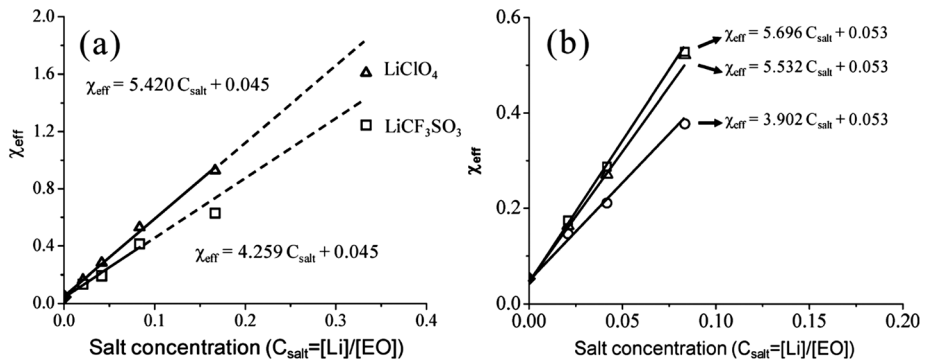

Fig. 1 (a) χ_{eff} *vs.* salt concentration ([Li]/[EO]) at 166 °C. The χ of the neat sample is obtained from literature. The χ_{eff} values for salt-doped samples are calculated using domain spacing data obtained from *in situ* SAXS experiments and the relationship between domain spacing and the strong segregation regime. The linear regression lines (solid lines) were fitted using only the cylinder-forming samples in each system, and the lines were force fit through the neat sample. The regression lines, based on the cylinder-forming data, are extended to the lamellae-forming samples (dash lines). (b) χ_{eff} *vs.* salt concentration ([Li]/[EO]) at 120 °C. The low salt concentration samples show that χ_{eff} for each salt-doped system has a linear relationship with the salt concentration, and the slope decreases from PS-PEO:$LiAsF_6$ (square) > PS-PEO:$LiClO_4$ (triangle) > PS-PEO:$LiCF_3SO_3$ (circle). Reprinted with permission from ref. 31. © American Chemical Society, 2009.

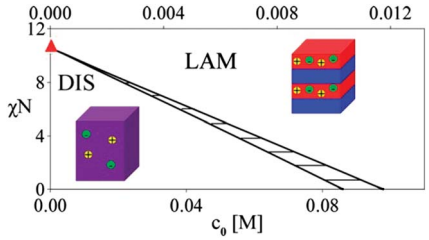

Fig. 2 Phase diagram containing the lamellar phase (LAM) and disordered phase (DIS). The shaded area indicates the phase coexistence. Reprinted with permission from ref. 37. © American Chemical Society, 2013.

sharp and broad peaks that persists in the temperature range, and the conductivity abruptly increases.[33,36] The phenomenon supports the scenario that the transition is first-order (the transition from the disordered state to the lamellar phase of salt-free AB block copolymers is second order) and the coexistence between the disordered phase and the lamellar phase in a finite range of temperature. Consistent with the experimental observations, in theory, Nakamura *et al.*[37] have recently shown that in the presence of lithium salts the disordered-to-lamellar phase transition becomes first-order even at the level of mean-field theory, with a moderate range of temperature in which both the disordered and lamellar phases coexist, and different salt concentrations in the coexisting phases. The coexistence arises from the different partitioning of the salt ions between the disordered phase and the lamellar phase, driven primarily by the solvation energy of anions. The simultaneous presence of sharp and broad scattering peaks in the SAXS measurements over a range of temperatures and the abrupt change in the ionic conductivity across the transition can be qualitatively explained by the finite temperature window of the transition at a fixed overall salt concentration shown by their phase diagram (Fig. 2).

2.2 Order–order transition (OOT)

The dynamical aspects of melt-phase behavior are also governed by interfacial reorganization. It has been recognized theoretically that interfacial fluctuations or corrugations play an important role in order–order transitions and set the kinetic pathway (or intermediate state).[38–40] Examples are shown in Fig. 3 for crystalline lamellar (k_1, k_2) to micellar (mc), hexagonal columnar (hex) to continuous cubic (cc), and cc to lamellar

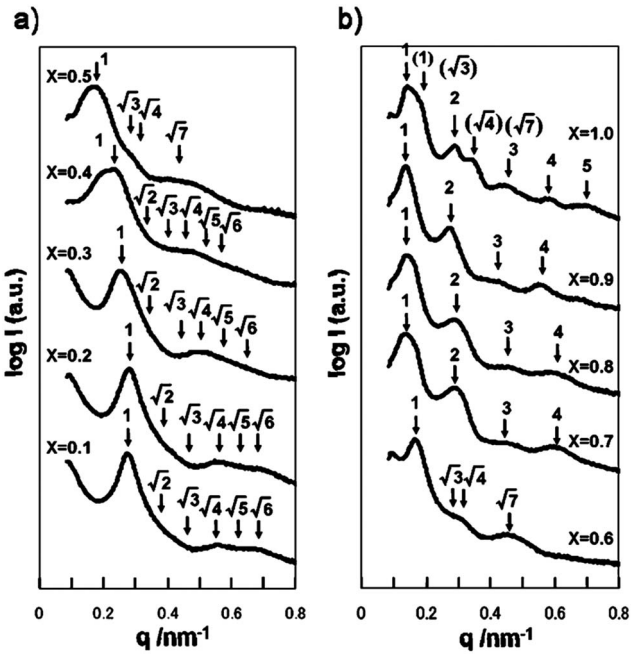

Fig. 4 SAXS profiles of Fe(*X*): (a) Fe(*X*) (X = 0.1–0.5); (b) Fe(*X*) (X = 0.6–1.0). Reprinted with permission from ref. 12. © American Chemical Society, 2010.

(lam) transitions.[41] Obviously, ion-doping stabilized the mesophases, resulting in a high-temperature shift of T_{OOT}. The stabilization of both the mc phase of Fig. 3a and the hex phase of Fig. 3b by about 50 °C can be attributed to the increased interaction parameter, χ, upon doping with lithium salts.

Small angle X-ray scattering (SAXS) and transmission electron microscopy (TEM) have been widely used for the quantitative analysis of OOT. In reciprocal space, the change in the position of the first-order scattering peak and higher order reflections should be monitored. In real space, TEM shows the mesophase transition more intuitional. For example, The OOT of polystyrene-*block*-poly (4-vinylpyridine) (PS-*b*-P4VP)/Fe^{3+} hybrid as a function of molar ratio of Fe^{3+} to 4VP was reported by Noro *et al.*[12] The SAXS profiles (Fig. 4) show a peak at the relative q position of 1, $2^{1/2}$, $3^{1/2}$, $4^{1/2}$, $5^{1/2}$, and $6^{1/2}$ at low salt concentration (molar ration smaller than 0.4), indicating bcc (body-center cubic) packing spheres. As for Fe(0.5) and Fe(0.6), the characteristic peaks shift to 1, $3^{1/2}$, $4^{1/2}$, and $7^{1/2}$, suggesting

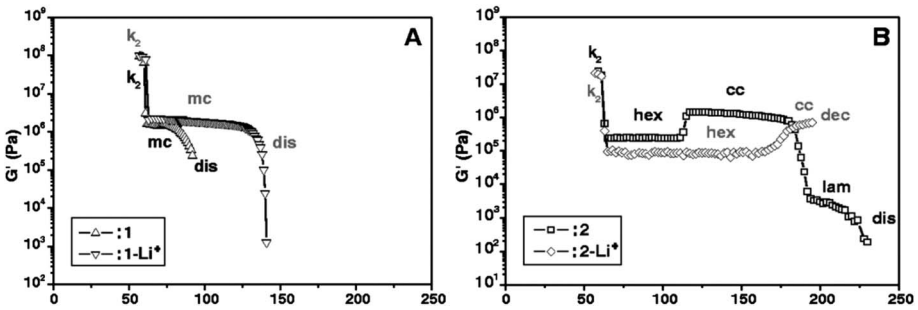

Fig. 3 Elastic modulus G' as a function of temperature for two compounds extended amphiphilic dendrons 1 and 2 and their ion-doped 1-Li^+ and 2-Li^+. Reprinted with permission from ref. 41. © *Science*, 2004.

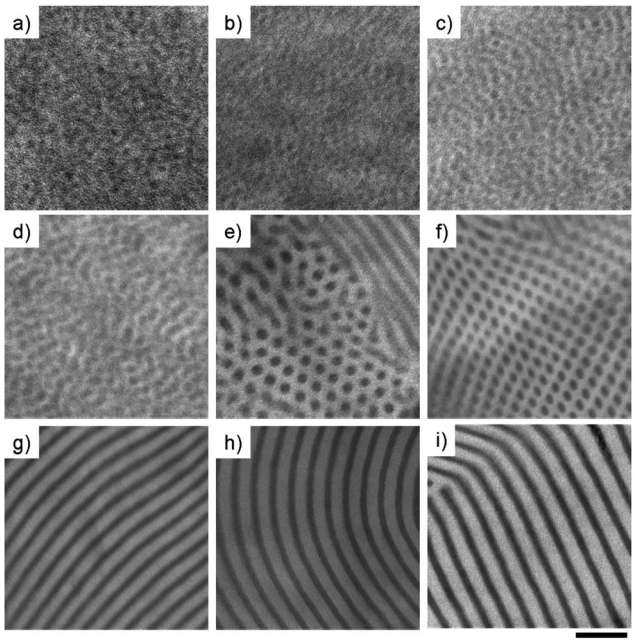

Fig. 5 TEM images of Fe(X) (X = 0.1–0.9): (a) Fe(0.1), (b) Fe(0.2), (c) Fe(0.3), (d) Fe(0.4), (e) Fe(0.5), (f) Fe(0.6), (g) Fe(0.7), (h) Fe(0.8), and (i) Fe(0.9). A scale bar represents 100 nm. Reprinted with permission from ref. 12. © American Chemical Society, 2010.

a cylinder structure, which coincided with the TEM results (Fig. 5). Finally, the structure turns to lamellar as peaks appear at q of 1, 2, 3, and 4. The intermediate composition in a morphological phase diagram appeared in the profile of Fe(0.4), which shows a quite broad peak possibly consisting of two peaks of spherical and cylinder structures. The identical result is shown in Fig. 5e.

A similar influence on the structure of microphase separation could be found in other salt doped systems. With increasing $LiClO_4$, a remarkable increase in χ along with a volumetric change produced by the selective coordination of $LiClO_4$ to P2VP block led to morphological transitions from disordered (dis) to bcc to hex to lam structures (Fig. 6).[42] For lithium doped PS-*b*-PI-*b*-PEO and PI-*b*-PS-*b*-PEO, two microstructures present in the neat material, core–shell gyroid (CSG) and semiperforated lamellae (SPL), are replaced by the core–shell cylinders (CSC) phase.[25,26] Wang *et al.* reported OOT from spheres to cylinders of lithium PS-*b*-PMMA complexes.[24] As PS-*b*-PEO doped with LiClO4 or $LiCF_3SO_3$, micromorphology transition from cylinders to lamellae were observed by SAXS.[31]

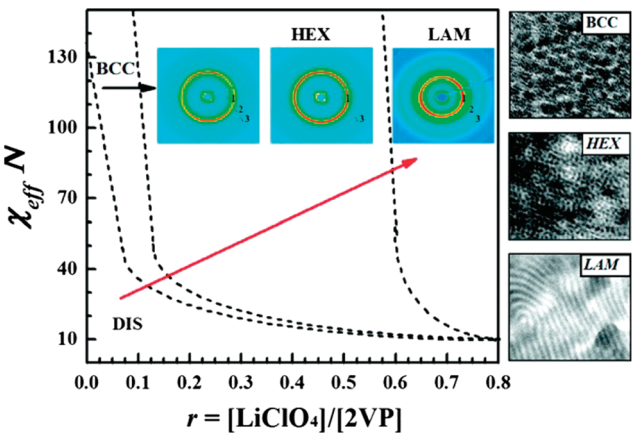

Fig. 6 Selective coordination of $LiClO_4$ to the ionophilic P2VP block led to morphological transitions from disordered (DIS) to body-centered cubic spherical (BCC) to hexagonally packed cylindrical (HEX) to lamellar (LAM) structures. Reprinted with permission from ref. 42. © American Chemical Society, 2011.

2.3 Disorder–order transition (DOT)

As described above, the phase behavior of flexible linear BCPs is dictated by the volume fraction of one block (f) and the product of χN. At low χN, the BCP is in the phase-mixed state, and as χN increases, it undergoes a disorder-to-order transition (DOT); that is, its microphase separates into ordered arrays of lamellar, hexagonally packed cylindrical, or body-centered cubic spherical microdomains or into a bicontinuous gyroid morphology, determined by the volume fraction of each component. Moreover, the DOT process can be induced or even controlled by the addition of salts. For instance, PS-*b*-PMMA, an ideal material to generate nanoporous templates, has a relatively weak non-favorable interaction between the PS and PMMA segments, making it difficult to achieve structural small features.[43] However, the low χ values can be significantly increased by incorporating additives that selectively associate with one block *via* specific interactions such as metal-ion coordination and hydrogen bonding.[13,24,28,44] Wang *et al.* reported that microphase separation can be induced by the addition of lithium salts to a phase mixed PS-*b*-PMMA.[24]

The DOT was further examined in films. It was found that significant orientation of lamellar microdomains parallel to the surface exists in ion-complex samples. Consequently, the copolymer has undergone a transition from a phase-mixed to a microphase-separated state with the formation of lithium-complexes, which originates from the integrated effect of the increase in segmental interactions, χ_{eff}, and the change in chain conformation. The DOT in BCPs films caused by ion coordination will be introduced below.

2.4 Domain spacing

Several studies on different ion-containing block copolymers have shown that the addition of salt also strongly changed the structural properties. In the ordered state, the addition of salt induced modifications of the phase behavior and large increases in the domain spacing (d). These changes were attributed to an increased value of the interaction parameter χ due to the added salt, and moreover based on the established relation $d \sim aN^{2/3}\chi^{1/6}$ (N is the degree of polymerization and a the segment length) which relates d with χ and is valid in the strong segregation limit.[25,26,31,45] Similar conclusions were drawn from temperature-dependent studies in the weak segregation regime showing increased domain spacings.[7,25,26,33] For pure block copolymers it is well-known that also in the weak segregation regime the domain spacing reflects the position of the peak in the structure factor ($d = 2\pi/q^*$) depending on the incompatibility. Thus, an increase of

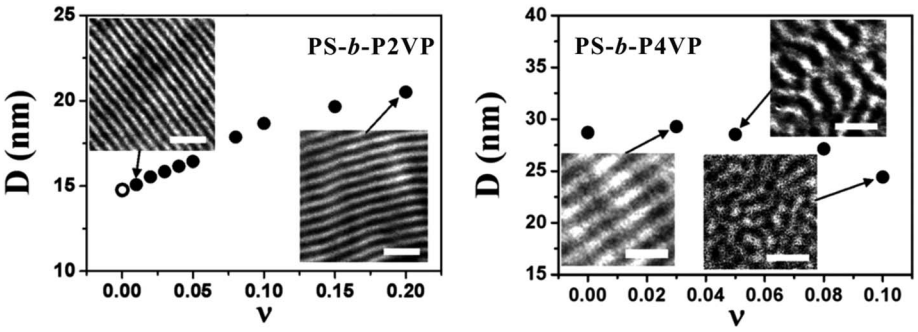

Fig. 7 Change of domain spacing (D) with the number of coordinated $CdCl_2$ per VP monomer unit (ν) for PS-P2VP and PS-P4VP. Inset TEM images (scale bar = 50 nm) are PS-P2VP[0.01], PS-P2VP[0.2], PS-P4VP[0.03], PS-P4VP[0.05], and PS-P4VP[0.1], respectively. Reprinted with permission from ref. 23. © American Chemical Society, 2006.

N and a decrease in temperature, leading to an increase of χ, were found to result in chain stretching.[46–49] On the other hand, the changes in structure can also be related to that in the conformation directly caused by coordination of ions with polymer chains. Lee *et al.*[22,23] presented strong evidence for such an effect. An increase or decrease in d was observed in cadmium-complexed polystyrene-*block*-poly(2-vinylpyridine) (PS-*b*-P2VP) and PS-*b*-P4VP copolymers, due to the different coordination type with cadmium ions (intra- *versus* intermolecular bridging coordination), instead of an increase in χ_{eff} (Fig. 7).[23] Similarly, d is effectively tuned by the amount of cadmium ion. Also, as a third point, it should be taken into account that the additional volume of the added salt leads to an increase of the domain spacing.[12,30,31]

In general, to distinguish the above-mentioned different possible causes for chain stretching is difficult. Gunkel *et al.* proposed and experimentally verified a reasonable assumption that also for ion-containing block copolymers the value of the incompatibility at the ODT is constant and, in particular, independent of salt concentration.[30] Thus, salt-induced changes of the domain spacing at the order–disorder transition should obey the following equation:

$$\frac{\mathrm{d}}{\mathrm{d}r}\mathrm{d}\left(\chi_{\mathrm{eff}}(r),\ r\right)\big|_{\mathrm{ODT}} = \frac{\partial}{\partial_{\chi_{\mathrm{eff}}}}\mathrm{d}\frac{\partial}{\partial_r}\chi_{\mathrm{eff}}\big|_{\mathrm{ODT}} + \frac{\partial}{\partial_r}\mathrm{d}\big|_{\mathrm{ODT}} \equiv \frac{\partial}{\partial_r}\mathrm{d}(r)\big|_{\mathrm{ODT}} \tag{4}$$

Here $(\partial\chi_{\mathrm{eff}}/\partial r)|_{\mathrm{ODT}} = 0$ according to the assumption $(\chi_{\mathrm{eff}}N)_{\mathrm{ODT}} = \mathrm{const}$. The remaining contribution $(\partial/\partial r)\mathrm{d}(r)|_{\mathrm{ODT}}$ represents that variation of d related to both conformational changes of the ion-containing blocks and changes due to the additional volume of the salt. Fig. 8 shows d at the corresponding T_{ODT} as a function of the molar ratio of $LiCF_3SO_3$ to 2VP and EO. The dashed lines were approximate calculations of the increase of d_{ODT} due to the volume of added salt. It was assumed that the volume of polymer and the volume of salt were simply additive in the mixture. In this case the increase of d due to the volume of added salt can be estimated as follows:

$$\frac{\mathrm{d}}{\mathrm{d}_{\mathrm{BCP}}} = 1 + \frac{V_{\mathrm{salt}}}{V_{\mathrm{BCP}}} = 1 + x_{\mathrm{m}}\frac{\rho_{\mathrm{BCP}}}{\rho_{\mathrm{salt}}} \tag{5}$$

Here d_{BCP} denotes the domain spacing in the neat block copolymer, V_{BCP} its volume and χ_{m} the mass ratio known for the sample preparation. As shown in Fig. 8, the increase of d_{ODT} coincided with the contribution of salt volume (dashed line) at low salt concentrations ($\approx$4% for 2VP and $\approx$1% for EO) and then increased strongly which could be attributed to salt-induced chain stretching. Thus, the salt-induced changes in domain spacing originate from the integrated effect of the increase of χ_{eff}, the salt volume contribution and the salt-induced chain stretching.

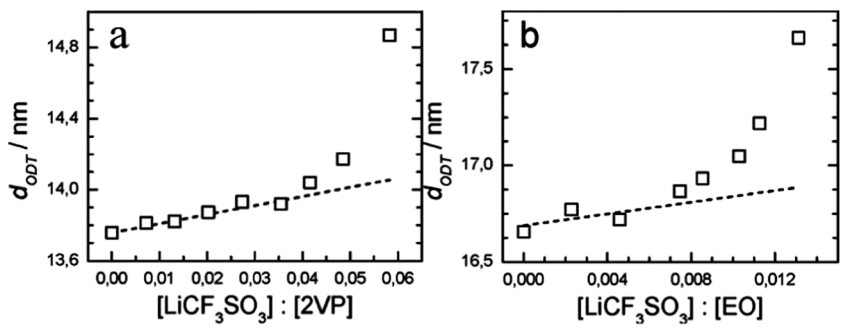

Fig. 8 The domain spacing $d = 2\pi/x_c$ at the corresponding T_{ODT} are shown *versus* the molar ratio of (a) $[LiCF_3SO_3]$: [2VP] and (b) $[LiCF_3SO_3]$: [EO]. The dashed line represents the estimated increase of the domain spacing due to the volume of the added salt. Reproduced with permission from ref. 30. © American Chemical Society, 2012.

3. Ion influence upon morphologies of BCPs thin films

The block copolymers are generally used as templates and scaffolds for the fabrication of nanostructured materials due to the microphase separation induced nanoscopic structures.[1,50,51] In addition to the previously mentioned driving forces that determine the bulk state phase behavior of block copolymers, two additional factors play a role in block copolymer thin films: the surface/interface energies as well as the interplay between the film thickness t and the natural period, L_0, of the bulk microphase-separated structures.[52–55] Strong preferential interactions of one block with the substrate or a lower surface energy of one component causes a segregation of that block to either the substrate interface or the surface of the film.[56] As a result, the connectivity of the blocks forces a parallel orientation of the microdomain to the substrate. The influence of the surface or interface on the orientation of BCPs microdomains rapidly decays with distance, so that a random orientation of the microdomains was observed at a distance corresponding to several repeated periods of the BCP in thick films.[57]

As is known, key for successfully realizing film utilization is the control of orientation and lateral ordering of the BCP microdomains. Hence, a number of strategies have been developed including either manipulating interfacial interactions by surface modification or overcoming the interfacial interactions by applying external fields, such as temperature gradient, mechanical flow field, solvent field, electric field and confinement effect. Theoretically, the orientation of lamellar microdomains in symmetric BCP thin films was observed taking account of the competition between the applied field, E_{app}, and surface interactions.[58,59] In the strong segregation regime, there are two critical fields E_1 and E_2 when there are strong, preferential interfacial interactions. For $E_{app} < E_1$, the lamellar microdomains orient parallel to the interfaces due to preferential interactions and for $E_{app} > E_2$, the microdomains orient normal to the interfaces. When $E_1 < E_{app} < E_2$, a mixed orientation of microdomains is predicted where the lamellar microdomains near the interfaces align with the planes of the interfaces and in the center of the film they orient in the direction of E_{app}.[60] Experimentally, Morkved *et al.* examined the effect of an electric field on PS-*b*-PMMA block copolymer thin film morphology. In-plane cylinders were found to be aligned parallel to the electric field lines after long annealing times.[61] Additionally, Xu *et al.*[62] put forward the competition between the applied electric field, aligning the microdomains normal to the surface, and surface fields that tend to align the microdomains parallel to the surface. For films with thickness $t < 10L_0$, interfacial interactions are dominant, and the lamellar microdomains orient parallel to the substrate surface

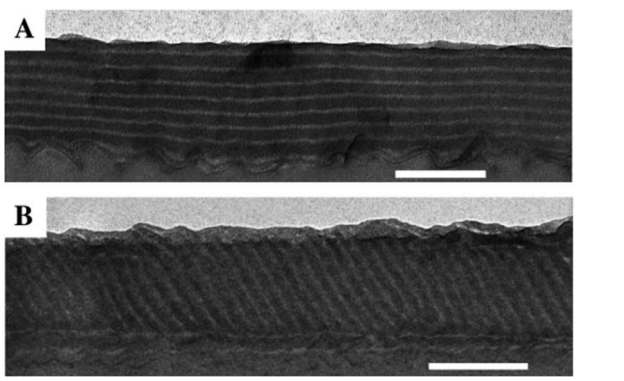

Fig. 9 Cross-sectional TEM images of (a) pure PS-*b*-PMMA thin film and (b) PS-*b*-PMMA copolymer thin film containing lithium complexes with a thickness of ~260 nm after applying a ~40 V μm^{-1} dc electric field at 175 ± 5 °C under N_2 for 20 h. Scale bar: 200 nm. Reprinted with permission from ref. 60. © American Physical Society, 2006.

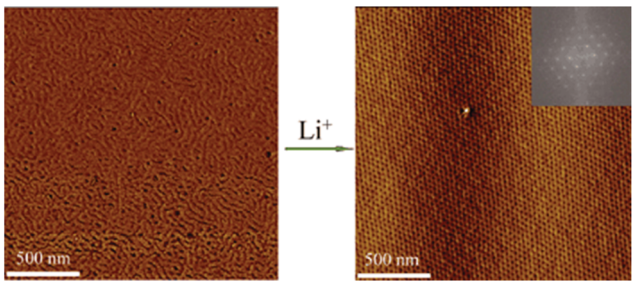

Fig. 10 SFM phase image of PS-*b*-P2VP without LiCl after annealing under saturated $CHCl_3$ vapor for 24 h. SFM phase images and their Fourier transforms (shown in the inset) of PS-*b*-P2VP with 1 wt% LiCl after annealing under saturated $CHCl_3$ vapor for 24 h. The phase ranges from 0° to 30° in all the images. Reprinted with permission from ref. 67. © Wiley, 2007.

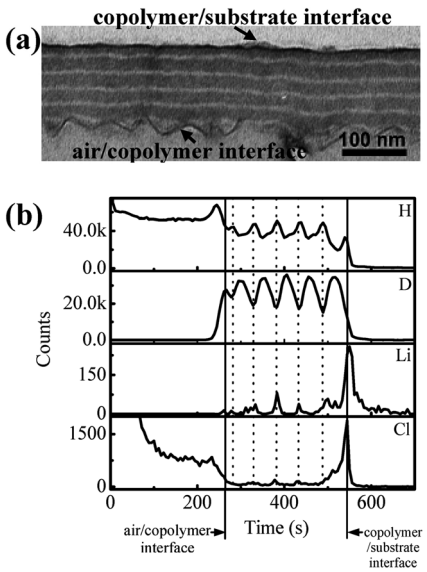

Fig. 11 (a) Cross-sectional TEM image of a dPS-*b*-PMMA (M_n 56 kg mol^{-1}) copolymer film with a thickness of ~190 nm, where ~13% of carbonyl groups complexed to lithium ions after being thermally annealed at 170 °C under vacuum for 2 days. (b) The corresponding dynamic SIMS profiles. H, hydrogen ion, characterizing PMMA microdomains; D, deuteron ion, characterizing dPS microdomains; Li, lithium ion; Cl, chlorine ions. For clarity, vertical solid lines are used to demark the copolymer/air interface (left) and copolymer/substrate interface (right) of the film and vertical dashed lines are used to demark the center of PMMA microdomains. Reprinted with permission from ref. 64. © American Chemical Society, 2008.

regardless of the applied electric field. If $t > 10L_0$, interfacial interactions become less important, and lamellar microdomains in the center of the films could be oriented in the direction of the applied field, namely, normal to the surface. However, only the domains in the center of the film turned, excluding the domains near the interface or surface. In other words, dielectric breakdown occurs before complete alignment is achieved in pure BCP films and only a mixed orientation is found.[63] It is proved that although the application of external fields is effective, it still remains a challenge in terms of the complete alignment of BCP microdomains normal to the surface.

It is known that the formation of ion BCPs complexes affects the immiscibility between the blocks and mediating the interfacial interaction. Russell's group found that the formation of lithium–PMMA complexes resulted in a significant increase of dielectric contrast which markedly reduced the critical electric field strength required to overcome the preferential interactions of one block with the substrate.[56] Wang *et al.*[45,64] proposed that adding LiCl salt into PS-*b*-PMMA copolymer films can direct the orientation of lamellar microdomains. By tuning the amount of ionic complexes, the orientation of lamellar microdomain can be controlled from a random arrangement to being oriented parallel or perpendicular to the film surface without any surface modification or external fields, which opens a facile and general route for the fabrication of nanostructured materials. Thus, for lithium–PMMA complexes thin films, both E_1 and E_2 decrease to values below the dielectric breakdown value of the copolymer. The alignment of the microdomains even near the surface can be achieved which can't be realized in pure PS-*b*-PMMA (Fig. 9).[60] Meanwhile, the contribution made by the "free-ion mechanism", which enhances the ability of the electric field to

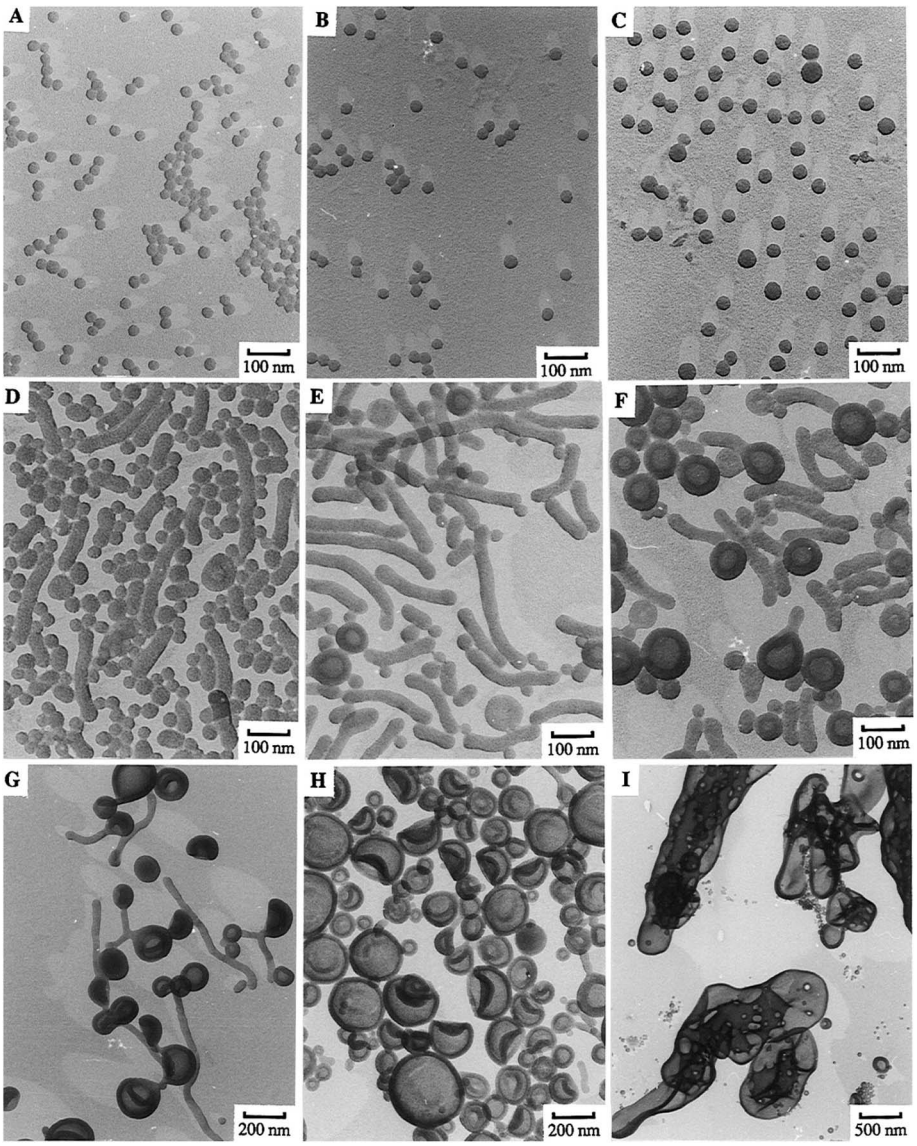

Fig. 12 Aggregates from PS(410)-*b*-PAA(25) without any additive (A) and with added NaCl to different final concentrations: (B) 1.1 mM ($R = 0.20$); (C) 2.1 mM ($R = 0.40$); (D) 3.2 mM ($R = 0.60$); (E) 4.3 mM ($R = 0.80$); (F) 5.3 mM ($R = 1.0$); (G) 10.6 mM ($R = 2.0$); (H) 16.0 mM ($R = 3.0$); (I) 21 mM ($R = 4.0$). Reprinted with permission from ref. 72. © American Chemical Society, 1996.

align diblock copolymer microdomains, should be taken into account.[65,66] Additionally, the reorganization of ion-containing BCP thin films in a solvent atmosphere are improved compared with the neat one. For Li^+ doped PS-*b*-P2VP, microdomains orient normal to the surface during solvent evaporation, enabling the fabrication of highly ordered structures over large areas.[67] By controlling the molar ratio of N : Li and solvent evaporation rate, hexagonally packed cylindrical microdomains with exceptionally long-range ordering have been obtained (Fig. 10). This approach provides an efficient and simple method for fabricating templates with ordered nanoscale structures for various applications. Results for PS-*b*-PEO, where PEO block doped with KI, showing similar behavior to that of PS-*b*-P2VP.[13] Considering the effect of noncomplexed salt, *i.e.*, physically mixed salts on the reorientation of microdomains, dynamic secondary ion mass spectrometry (DSIMS) was used to investigate the distribution of added salt in the thin film (Fig. 11).[64] It is most likely that noncomplexed salts, preferentially locate at the copolymer/substrate interface and act to mediate interfacial interactions. Furthermore, the transition metal ions doped BCPs can be converted into the corresponding metallic nanoparticles by reduction reactions, providing a simple route for the incorporation of inorganic nanoparticles into BCPs microdomains.[68–71]

In conclusion, the added salts selectively locate on one block of BCPs, which enhances the immiscibility of the blocks, mediates the interfacial interaction and enlarges the dielectric contrast, opening up a simple and general route for the fabrication of long-range ordering nanostructured materials without any surface modification. Therefore, this general strategy allows one to generate functional, self-orienting, self-assembling systems that hold promise in the fabrication of nanostructured materials where the spatial placement of each element can be controlled and, as such, opens a pathway to addressable media.

4. Ion influence upon self-assembly behavior of BCPs in solutions

The self-assembly of amphiphilic block copolymers in solutions has attracted much attention in the past few decades. Studies on the ion-induced morphological changes of block polymer assemblies can be traced back to the Eisenberg group.[10,72] For a diblock copolymer of polystyrene-*b*-poly(acrylic acid) (PS-*b*-PAA), morphological changes can be induced by the addition of ions in micromolar ($CaCl_2$ or HCl) or millimolar (NaCl) concentrations. In addition to spherical, rod-like, and univesicular or lamellar aggregates, large compound vesicle (LCVs) morphologies were obtained from a single block, which are useful as drug-delivering vehicles and as models of stable microstructured biomaterials (Fig. 12).[72] The morphologies are the same as those produced by changes in the copolymer composition in the absence of added ions, which suggests that the morphological changes are probably induced by decreased repulsion (both steric and electrostatic) among the hydrophilic

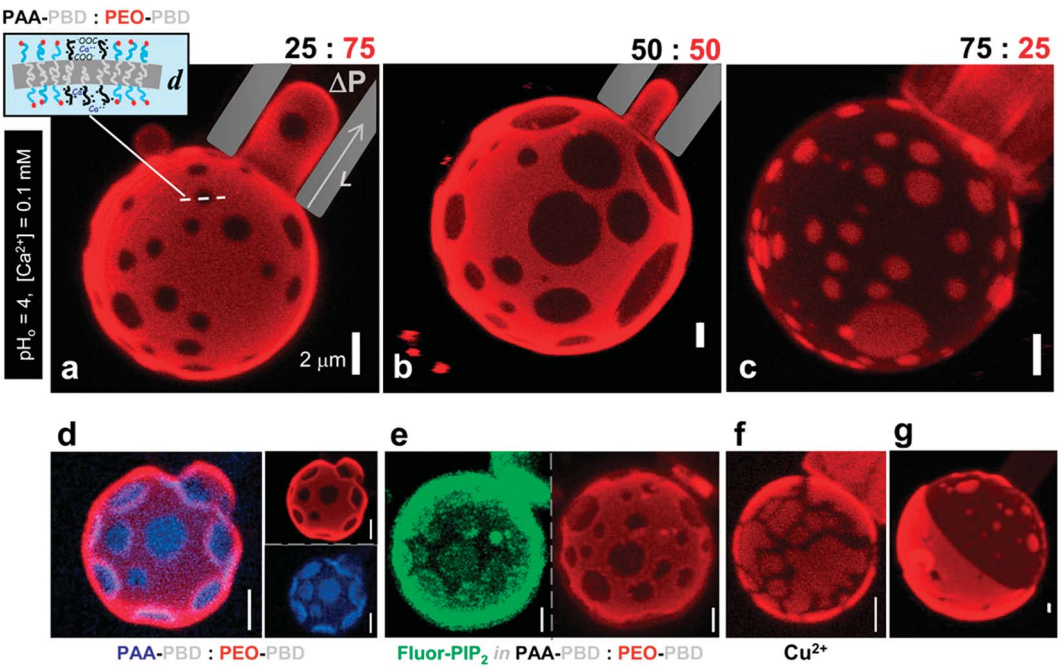

Fig. 13 Cation-induced, lateral phase segregation of charged PAA-PBD and neutral, fluorescently labeled PEO-PBD* diblock copolymers formed at pH_0 4, 0.1 mM calcium at (a) 25% PAA-PBD, (b) 50% PAA-PBD, and (c) 75% PAA-PBD. (a, inset): schematic of phase-separated membrane of thickness *d*. (d) Two color micrograph of a phase separated polymersome (34% PAA-PBD, PAA-PBD : PAA-PBD* = 10 : 1) with individual red (PEO-PBD*) and blue (PAA-PBD*) channel micrographs to illustrate the extent of demixing. (e) Individual channels modified using an averaging smoothing filter to enhance contrast for a two color phase separated polymersome (50% PAA-PBD) with 2% PIP2-BodipyFL (green) enriched in dark PAA-PBD domains and partially segregated from the PEO-PBD*-rich domains (red). (f) Phase separation of PAA-PBD (50%) induced by copper(II) at pH_0 3.5, 0.075 mM copper(II). (g) Janus polymersome resulting from domain coarsening in a 50% PAA-PBD polymersome. Reprinted with permission from ref. 76. © Nature Publishing Group, 2009.

segments as a result of protonation or of ion binding or bridging. Whereas, the newly discovered LCVs are from the kinetic control, involving collisions of vesicles and a subsequent fusion process.[73] It also demonstrated that divalent cations, such as $CuCl_2$, can promote the bump formation on assembled nanospheres from a block copolymer with a polyanionic block, and thus gave particles with segregated surface chains.[74] In addition, Guillet *et al.*[75] found the size, conformation, and functionality of coronal chains in polymeric micelles of terpyridine end-capped polystyrene-*b*-poly(*tert*-butylacrylate) (PS-*b*-PtBA) could be tuned by metal–ligand interactions, resulting in the formation of flower-like micelles. In this system, corona engineering is accomplished by affecting terpyridine-bearing chains in the presence of ionic stimuli, such as Ni^{2+}, Zn^{2+}, and Fe^{2+}. Recently, Discher's group reported the facile creation of spotted vesicles, striped cylinder micelles, and Janus assemblies, from mixtures of polyvalent amphiphiles, which are achieved by selective binding of multivalent ligands with cations such as Ca^{2+} or Cu^{2+}.[76] One of the amphiphilic block polymers yields polymersomes and micelles as a function of pH and salt concentration, while the other forms both cylinders and vesicles independent of the solution conditions. The co-assembly of these two block copolymers produced giant vesicles. Upon introducing Ca^{2+}, spotted vesicles were obtained, with their segregated domain size depending on the mixing ratio. In addition to the composition of copolymer mixtures, the domain size can be modulated by the hydration time. Moreover, controlled coarsening can yield Janus-like polymersomes (Fig. 13). Since the generality of this strategy has been assessed by introducing lipid phosphatidylinositol-4,5-bisphosphate (PIP2) or using another divalent cation Cu^{2+}, it provides a flexible and diverse structural control in a wide range of systems by different multivalent metal cations or chelating agents. This progress opens up a facile route to dynamic control over structural reorganization and functionalization with supermolecular assemblies. In addition, the novel assemblies decorated with cation-crossbridged microdomains of block copolymers play an important role in selective entrapment/release of therapeutics for gene therapy or drug delivery.[77] Besides the assemblies constructed from amphiphiles bearing ionic segments, introducing inorganic or organic salts may lead to the morphological transformation of nanostructures assembled from coordination polymers and copolymers with neutral hydrophilic segments.[10,78,79]

In short, understanding structural transitions of block polymer assemblies in the presence of various ions in solution are of fundamental importance, and ions are able to regulate the size and morphology of complex structures.

5. Ion influence upon application of solid polymer electrolytes

The urgent need for batteries with high power and energy densities increases the demand for advanced solid-state batteries due to their numerous desirable features including high energy density, good mechanical stability, and solvent free composition. A key component of these batteries is the electrolyte that facilitates ion transport between electrodes, and dry electrolyte systems with high mechanical strength which are advantageous for avoiding thermal runaway reactions and dendrite formation during repeated charge–discharge cycles.[80] Polymers that dissolve lithium ions are promising electrolyte materials for the next generation of rechargeable batteries.[81–86] But despite decades of research, two major problems prevent their implementation: (1) dendrite growth resulting in battery failure and (2) low conductivity at room temperature.[11] Theoretical work predicted that dendrite growth can only be completely suppressed by an electrolyte with a shear modulus near 6 GPa.[87] However, practical applications have been limited to the use of liquid-state electrolytes to ensure efficient ion transport, which typically exhibit shear moduli well below 1 MPa. In order to conduct ions while inhibiting dendrite growth, the shear modulus of solid polymer electrolytes must be increased by several orders of magnitude without significantly impairing ion transport.[11] Numerous attempts have been made to increase polymer shear modulus, either cross-linking the conductive homopolymer[88,89] or using inorganic fillers,[90] and block copolymers with well-defined ion-conducting pathways and a relatively high shear modulus were considered to have the potential to overcome the thermal and mechanical limitations of current electrolyte systems.[85,91] The potential of block copolymers to resolve the conflicting demands between high conductivity and high modulus has been recognized in several previous studies.[31,33,82,91–94]

With high ion solubilities and low T_g,[95,96] lamellar PS-*b*-PEO block copolymers containing lithium salts have been the most popular system. The mechanical properties are dominated by the rigid PS block, whereas the conductivity depends crucially on the connectivity of the PEO domains where the ions reside. As is known, the performance of electrolytes in batteries depends on multiple properties, for example, the conductivity, shear moduli, salt diffusion coefficient, the activity coefficient in the electrolyte and the cation transference number.[97] Numerous studies were carried out on these properties. Simultaneously, the relationship between chain conformations and coordination of Li^+ ions with PEO homopolymer chains were studied by molecular dynamics (MD) simulations,[98,99] showing that lithium is better coordinated by chains in a non-extended conformation. Experimentally, it has been determined that the conductivity of (PS-*b*-PEO)–salt mixtures increases with the molecular weight of the copolymers and reaches a plateau when the copolymer molecular weight approaches 100 kg mol^{-1}.[85] The long-range order of the copolymers appears to decrease with increasing molecular weight, but annealing has no effect on the ionic conductivity as reported, suggesting that long-range order does not affect conductivity.[92,98] Although the conductivities of lamellar PS-*b*-PEO copolymers is lower than that of pure PEO, it exhibits shear moduli that are orders of magnitude higher than those of PEO.[85,91] Besides, Energy Filtered Transmission Electron Microscopy (EFTEM) results show that the salt is increasingly localized in the middle of the PEO lamellae as the molecular weight of the copolymers increased due to nonuniform local stresses in the lamellae and the coupling between Li^+ coordination and these stresses.[92]

Such a distribution of ions in the polymer matrix would improve the properties and performance of a variety of devices.[80,96,100–102] Mullin *et al.* measured the salt diffusion coefficient of a series of nanostructured block copolymer electrolytes in a symmetric lithium/polymer electrolyte/lithium cell using the restricted diffusion technique. The average diffusion coefficient (D_{avg}) of the (PS-*b*-PEO)–LiTFSI mixtures increases with increasing molecular weight of the PEO block, M_{PEO}, and reaches a plateau of $2/3D_{PEO}$ when M_{PEO} exceeds 50 kg mol^{-1} (D_{PEO} is the average salt diffusion coefficient in PEO homopolymer).

Aiming at low conductivity at room temperature, Young[32] found a simple, yet effective, mixed-salt method to enhance the room temperature ionic conductivity of lithium-doped block copolymer electrolyte membranes by suppressing the crystalline phases in the conducting block. These electrolyte systems are especially suitable in solid-state lithium batteries, where a thermally, electrochemically, and mechanically stable electrolyte membrane with high ionic conductivity over a wide temperature range is needed (Fig. 14). The researchers examined a mixed-salt system of $LiClO_4$ and LiTFSI doped into a lamellae-forming PS-*b*-PEO diblock copolymer. The melting temperatures and degrees of crystallinity of the crystalline phases could be decreased in the PS-*b*-PEO system at [EO] : [Li] = 6 : 1. The reduction of melting temperature and crystallinity enabled one to obtain higher ionic conductivities at low temperatures compared to the corresponding single-salt-doped PS-*b*-PEO electrolytes. Additionally, they examined the mixed-salt and salt concentration effects on block copolymer energetic, proving the close Lewis acidities of LiTFSI and $LiClO_4$ as previously postulated.[32]

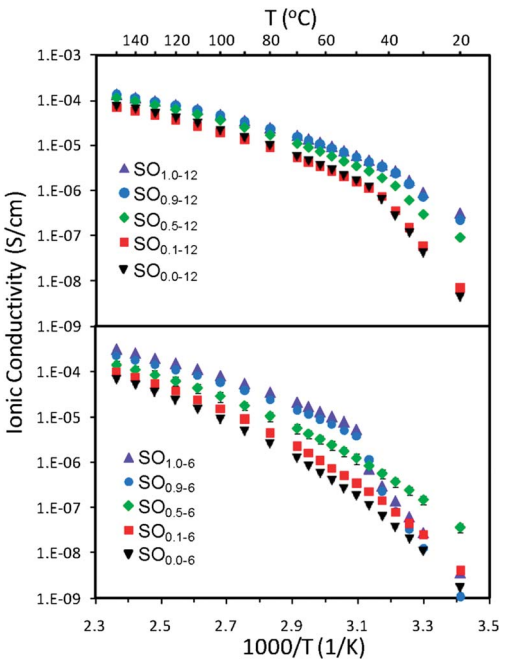

Fig. 14 Ionic conductivity profiles of salt-doped PS-*b*-PEO samples at [EO] : [Li] = 12 : 1 (upper panel) and 6 : 1 (lower panel). Samples were annealed at 150 °C for 2 h and then cooled to 20 at 30 °C min^{-1} and held for 12 h before measurement on heating. The annealing time before each measurement was 5 min. The reported values are the average of multiple samples at each mixed-salt and salt-doping ratio, and the typical standard deviation is shown on the data for $SO_{0.5-6}$. Samples are denoted as $SO_{x.x-y}$, where *x.x* represents the mixed-salt ratio ([LiTFSI]/([LiTFSI] + [$LiClO_4$]) = *x.x* = 0.0, 0.1, 0.5, 0.9, or 1.0) and *y* represents the salt-doping ratio. Reprinted with permission from ref. 32. © American Chemical Society, 2011.

Meanwhile, other types of block copolymer electrolytes–lithium batteries have also shown great progress. Javier reported[103] a new type of lithium battery in which a cathode with $LiFePO_4$ particles dispersed in a solid polymer electrolyte poly(3-hexylthiophene)-*b*-poly(ethylene oxide) (P3HT-PEO) and lithium metal anodes were assembled. In contrast to previous lithium battery electrodes, one material used in such a system served as the binder and transporter of electronic charge and lithium ions. The polymer was used in a battery cathode, and cycling experiments demonstrated that P3HT-PEO delivers both ions and electronic charge to the active centers. All of the supporting functions required in a battery electrode are thus performed by a single material. Furthermore, it was found that the addition of a lithium salt increases microphase separation and enhances the ordering in P3HT-PEO bulk samples.

Another attractive way of developing solid-state electrolytes that has received enormous interest in recent years is using ionic liquids. Ionic liquids, composed of organic cations and counterions, reveal fascinating physicochemical properties such as large thermal and electrochemical stability windows and negligible vapor pressure. They have particularly emerged as important materials in the era of electrochemistry owing to the prospects of offering efficient ion conduction and can be used as powerful electrolytes in diverse electrochemical devices.[104] The essential requisite of ionic liquid incorporated polymer electrolytes for their use in lithium batteries is to achieve high Li^+ conductivity, which is intimately related to the specific energy and the lithium storage capacity of the batteries. Thus, the extensive researches on ionic liquid incorporated polymer electrolytes have focused on the achievement of high ion conductivity by combining various kinds of ionic liquids and different polymers.[105] As expected and reported by many researchers, the addition of ionic liquids into polymer electrolytes results in increasing Li^+ conductivity, because the ionic liquid serves as a plasticizer to speed up the relaxation of the polymer chains, namely, the lowering of the glass transition temperature of the polymer.[106] The common cations in ILs fall into one of the following three types: alkyl imidazoliums, alkyl pyrrolidiniums, and alkyl sulfoniums. The categories of anions vary.[107] When the above-mentioned ionic liquids were incorporated into Li^+ doped polymer electrolytes, an improved conductivity range from 10^{-4} to 10^{-3} was achieved. It breaks the well-known conductivity limits of solid polymer electrolytes[96] but is still lower than that of conventional liquid electrolytes. The key parameter to improve the Li^+ conductivity is to increase the transport properties, which is closely related to the types of cations and anions in the ionic liquid. Park *et al.*[106] recently investigated the morphologies and electrochemical properties of ionic liquid incorporated PS-*b*-PEO electrolytes. Accompanied by the enhanced segregation strength between the ion-containing PEO domains and the nonconducting PS domains, the incorporation of small amounts of ionic liquids (10 wt%) resulted in significant increment (3–5 times) in the ionic

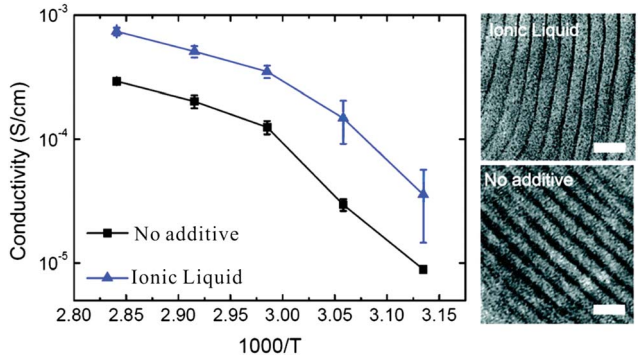

Fig. 15 The temperature-dependent ionic conductivity of Li salt-doped PS-*b*-PEO block copolymer electrolytes in the presence and absence of ionic liquids. Reproduced with permission from ref. 106. © American Chemical Society, 2011.

conductivity, as shown in Fig. 15. They attributed this to the exclusion of ionic liquids by the nonconductive PS domains, which eventually produced the higher local ionic liquid concentration in the conductive PEO domains and facilitated fast ion transport.

In brief, although solid-state electrolytes major limitation, its fascinating future prospects drive the development of solid electrolytes that can replace liquid electrolytes in lithium batteries. This development will satisfy the need to improve the safety, simplify the manufacturing process with flexible design, and achieve electrochemical stability at high cell potential. Moreover, it also provides exciting possibilities for the development of future high-energy lithium batteries by enabling the direct use of lithium metal at the anode.

6. Summary and outlook

Recent research efforts demonstrated the utility of ion/BCP hybrids as components in a new generation of BCP assemblies, film lateral ordering, BCP electrolytes, *etc.* The ionic complexes offer unprecedented influence on the phase behavior of BCP with an ion-dissolving block. The process of DOT, OOT and ODT in bulk can be achieved by simply controlling the ion component, concentration, *etc.* without changing the BCP chemical structures. Moreover, for BCP films, the added salts which selectively locate on one block of BCP enhancing the immiscibility of the blocks, mediating the interfacial interaction and enlarging the dielectric contrast, open up a simple and general route for the fabrication of long-range ordered nanostructured materials without any surface modification. On that basis, elegant methods of harnessing the microphase separation to produce ordered dispersions of inorganic nanoparticles have been developed. Significant advances in polymer electrolytes have been made by BCPs, depending on their well-defined ion-conducting pathways and a relatively high shear modulus. Such behavioral control, necessary in any application, evolved directly from research on the fundamental physics, chemistry and engineering of BCPs. The addition of ions makes it possible to incorporate different functionalities into BCPs, offering a route for further applications such as luminescent, electric, magnetic, and nonlinear optical materials.

Acknowledgements

This work was supported by the National Natural Science Foundation of China (20974077).

References

1 T. P. Lodge, *Macromol. Chem. Phys.*, 2003, **204**, 265–273.
2 F. S. Bates and G. H. Fredrickson, *Annu. Rev. Phys. Chem.*, 1990, **41**, 525–557.
3 G. Holden, N. R. Legge, R. Quirk and H. E. Schroeder, *Thermoplastic Elastomers*, Hanser Publishers, New York, 2nd edn, 1996.
4 G. S. MacGlashan, Y. G. Andreev and P. G. Bruce, *Nature*, 1999, **398**, 792–794.
5 Z. Gadjourova, Y. G. Andreev, D. P. Tunstall and P. G. Bruce, *Nature*, 2001, **412**, 520–523.
6 R. P. Pereira, A. M. Rocco and C. Bielschowsky, *J. Phys. Chem. B*, 2004, **108**, 12677–12684.
7 A. V. G. Ruzette, P. P. Soo, D. R. Sadoway and A. M. Mayes, *J. Electrochem. Soc.*, 2001, **148**, A537–A543.
8 A. M. Christie, S. J. Lilley, E. Staunton, Y. G. Andreev and P. G. Bruce, *Nature*, 2005, **433**, 50–53.
9 D. R. Sadoway, B. Huang, P. E. Trapa, P. P. Soo, P. Bannerjee and A. M. Mayes, *J. Power Sources*, 2001, **97–98**, 621–623.
10 L. Zhang, K. Yu and A. Eisenberg, *Science*, 1996, **272**, 1777–1779.
11 S. A. Mullin, G. M. Stone, A. Panday and N. P. Balsara, *J. Electrochem. Soc.*, 2011, **158**, A619–A627.
12 A. Noro, Y. Sageshima, S. Arai and Y. Matsushita, *Macromolecules*, 2010, **43**, 5358–5364.
13 S. H. Kim, M. J. Misner, L. Yang, O. Gang, B. M. Ocko and T. P. Russell, *Macromolecules*, 2006, **39**, 8473–8479.
14 J. P. Spatz, T. Herzog, S. Mößmer, P. Ziemann and M. Möller, *Adv. Mater.*, 1999, **11**, 149–153.
15 M. Breulmann, S. Förster and M. Antonietti, *Macromol. Chem. Phys.*, 2000, **201**, 204–211.
16 B. H. Sohn, S. I. Yoo, B. W. Seo, S. H. Yun and S. M. Park, *J. Am. Chem. Soc.*, 2001, **123**, 12734–12735.
17 R. Glass, M. Möller and J. P. Spatz, *Nanotechnology*, 2003, **14**, 1153.
18 H. G. Boyen, G. Kästle, K. Zürn, T. Herzog, F. Weigl, P. Ziemann, O. Mayer, C. Jerome, M. Möller and J. P. Spatz, *Adv. Funct. Mater.*, 2003, **13**, 359–364.
19 I. W. Hamley, *The physics of block copolymers*, Oxford University Press New York, 1998.
20 F. Bates and G. Fredrickson, *Phys. Today*, 1999, **52**, 32.
21 J. K. Kim, J. I. Lee and D. H. Lee, *Macromol. Res.*, 2008, **16**, 267–292.
22 D. H. Lee, S. H. Han, W. Joo, J. K. Kim and J. Huh, *Macromolecules*, 2008, **41**, 2577–2583.
23 D. H. Lee, H. Y. Kim, J. K. Kim, J. Huh and D. Y. Ryu, *Macromolecules*, 2006, **39**, 2027–2030.
24 J. Y. Wang, W. Chen, C. Roy, J. D. Sievert and T. P. Russell, *Macromolecules*, 2008, **41**, 963–969.
25 T. H. Epps III, T. S. Bailey, H. D. Pham and F. S. Bates, *Chem. Mater.*, 2002, **14**, 1706–1714.

26 T. H. Epps III, T. S. Bailey, R. Waletzko and F. S. Bates, *Macromolecules*, 2003, **36**, 2873–2881.
27 I. Nakamura and Z.-G. Wang, *Soft Matter*, 2012, **8**, 9356–9367.
28 J. Y. Wang, W. Chen and T. P. Russell, *Macromolecules*, 2008, **41**, 4904–4907.
29 N. S. Wanakule, J. M. Virgili, A. A. Teran, Z. G. Wang and N. P. Balsara, *Macromolecules*, 2010, **43**, 8282–8289.
30 I. Gunkel and T. Thurn-Albrecht, *Macromolecules*, 2012, **45**, 283–291.
31 W. S. Young and T. H. Epps III, *Macromolecules*, 2009, **42**, 2672–2678.
32 W. S. Young, J. N. L. Albert, A. B. Schantz and T. H. Epps III, *Macromolecules*, 2011, **44**, 8116–8123.
33 N. S. Wanakule, A. Panday, S. A. Mullin, E. Gann, A. Hexemer and N. P. Balsara, *Macromolecules*, 2009, **42**, 5642–5651.
34 Z. G. Wang, *J. Phys. Chem. B*, 2008, **112**, 16205–16213.
35 I. Nakamura, N. P. Balsara and Z.-G. Wang, *Phys. Rev. Lett.*, 2011, **107**, 198301.
36 A. A. Teran, S. A. Mullin, D. T. Hallinan Jr and N. P. Balsara, *ACS Macro Lett.*, 2012, **1**, 305–309.
37 I. Nakamura, N. P. Balsara and Z.-G. Wang, *ACS Macro Lett.*, 2013, **2**, 478–481.
38 M. Laradji, A. C. Shi, R. C. Desai and J. Noolandi, *Phys. Rev. Lett.*, 1997, **78**, 2577–2580.
39 C. Y. Ryu, M. E. Vigild and T. P. Lodge, *Phys. Rev. Lett.*, 1998, **81**, 5354–5357.
40 J. K. Kim, H. H. Lee, Q. J. Gu, T. Chang and Y. H. Jeong, *Macromolecules*, 1998, **31**, 4045–4048.
41 B. K. Cho, A. Jain, S. M. Gruner and U. Wiesner, *Science*, 2004, **305**, 1598–1601.
42 S. Naidu, H. Ahn, J. Gong, B. Kim and D. Y. Ryu, *Macromolecules*, 2011, **44**, 6085–6093.
43 X. Wei, L. Li, J. P. Kalish, W. Chen and T. P. Russell, *Macromolecules*, 2011, **44**, 4269–4275.
44 U. Jeong, D. Y. Ryu, D. H. Kho, D. H. Lee, J. K. Kim and T. P. Russell, *Macromolecules*, 2003, **36**, 3626–3634.
45 J. Y. Wang, J. M. Leiston-Belanger, J. D. Sievert and T. P. Russell, *Macromolecules*, 2006, **39**, 8487–8491.
46 B. Holzer, A. Lehmann, B. Stühn and M. Kowalski, *Polymer*, 1991, **32**, 1935–1942.
47 J. H. Rosedale, F. S. Bates, K. Almdal, K. Mortensen and G. D. Wignall, *Macromolecules*, 1995, **28**, 1429–1443.
48 N. Sakamoto and T. Hashimoto, *Macromolecules*, 1995, **28**, 6825–6834.
49 K. Almdal, K. Mortensen, A. J. Ryan and F. S. Bates, *Macromolecules*, 1996, **29**, 5940–5947.
50 M. Li, C. A. Coenjarts and C. K. Ober, in *Block Copolymers II*, Springer, 2005, pp. 183–226.
51 C. J. Hawker and T. P. Russell, *MRS Bull.*, 2005, **30**, 952–966.
52 T. P. Russell, G. Coulon, V. Deline and D. Miller, *Macromolecules*, 1989, **22**, 4600–4606.
53 A. Menelle, T. Russell, S. Anastasiadis, S. Satija and C. Majkrzak, *Phys. Rev. Lett.*, 1992, **68**, 67–70.
54 P. Mansky, Y. Liu, E. Huang, T. P. Russell and C. J. Hawker, *Science*, 1997, **275**, 1458–1460.
55 D. Y. Ryu, K. Shin, E. Drockenmuller, C. J. Hawker and T. P. Russell, *Science*, 2005, **308**, 236–239.
56 O. K. C. Tsui, *Polymer thin films*, World Scientific Publishing Company Incorporated, 2008.
57 T. Xu, C. J. Hawker and T. P. Russell, *Macromolecules*, 2005, **38**, 2802–2805.
58 G. Pereira and D. Williams, *Macromolecules*, 1999, **32**, 8115–8120.
59 Y. Tsori and D. Andelman, *Macromolecules*, 2002, **35**, 5161–5170.
60 J. Y. Wang, T. Xu, J. M. Leiston-Belanger, S. Gupta and T. P. Russell, *Phys. Rev. Lett.*, 2006, **96**, 128301.
61 T. L. Morkved, M. Lu, A. M. Urbas, E. E. Ehrichs, H. M. Jaeger, P. Mansky and T. P. Russell, *Science*, 1996, **273**, 931–933.
62 T. Xu, Y. Q. Zhu, S. P. Gido and T. P. Russell, *Macromolecules*, 2004, **37**, 2625–2629.
63 T. Xu, C. J. Hawker and T. P. Russell, *Macromolecules*, 2003, **36**, 6178–6182.
64 J. Y. Wang, W. Chen, J. D. Sievert and T. P. Russell, *Langmuir*, 2008, **24**, 3545–3550.
65 Y. Tsori, F. Tournilhac and L. Leibler, *Macromolecules*, 2003, **36**, 5873–5877.
66 Y. Tsori, F. Tournilhac, D. Andelman and L. Leibler, *Phys. Rev. Lett.*, 2003, **90**, 145504.
67 J. He, J. Y. Wang, J. Xu, R. Tangirala, D. Shin, T. P. Russell, X. Li and J. Wang, *Adv. Mater.*, 2007, **19**, 4370–4374.
68 S. Park, J. Y. Wang, B. Kim and T. P. Russell, *Nano Lett.*, 2008, **8**, 1667–1672.
69 S. Park, B. Kim, J. Y. Wang and T. P. Russell, *Adv. Mater.*, 2008, **20**, 681–685.
70 S. H. Yun, S. I. Yoo, J. C. Jung, W. C. Zin and B. H. Sohn, *Chem. Mater.*, 2006, **18**, 5646–5648.
71 S.-M. Jeon, S. H. Lee, S. I. Yoo and B.-H. Sohn, *Langmuir*, 2011, **27**, 12191–12196.
72 L. Zhang and A. Eisenberg, *Macromolecules*, 1996, **29**, 8805–8815.
73 H. Shao and J. R. Parquette, *Angew. Chem., Int. Ed.*, 2009, **48**, 2525–2528.
74 R. Zheng, G. Liu and X. Yan, *J. Am. Chem. Soc.*, 2005, **127**, 15358–15359.
75 P. Guillet, C. A. Fustin, C. Mugemana, C. Ott, U. S. Schubert and J. F. Gohy, *Soft Matter*, 2008, **4**, 2278–2282.
76 D. A. Christian, A. Tian, W. G. Ellenbroek, I. Levental, K. Rajagopal, P. A. Janmey, A. J. Liu, T. Baumgart and D. E. Discher, *Nat. Mater.*, 2009, **8**, 843–849.
77 J. Zhang and X. Li, *Prog. Polym. Sci.*, 2012, **37**, 1130–1176.
78 W. N. He, J. T. Xu, B. Y. Du, Z. Q. Fan and X. Wang, *Macromol. Chem. Phys.*, 2010, **211**, 1909–1916.
79 H. J. Kim, J. H. Lee and M. Lee, *Angew. Chem.*, 2005, **117**, 5960–5964.
80 J. Tarascon and M. Armand, *Nature*, 2001, **414**, 359–367.
81 F. Gray, J. MacCallum, C. Vincent and J. Giles, *Macromolecules*, 1988, **21**, 392–397.
82 B. K. Cho, A. Jain, S. Gruner and U. Wiesner, *Science*, 2004, **305**, 1598–1601.

83 P. P. Soo, B. Huang, Y. I. Jang, Y. M. Chiang, D. R. Sadoway and A. M. Mayes, *J. Electrochem. Soc.*, 1999, **146**, 32–37.
84 P. E. Trapa, Y. Y. Won, S. C. Mui, E. A. Olivetti, B. Huang, D. R. Sadoway, A. M. Mayes and S. Dallek, *J. Electrochem. Soc.*, 2005, **152**, A1–A5.
85 M. Singh, O. Odusanya, G. M. Wilmes, H. B. Eitouni, E. D. Gomez, A. J. Patel, V. L. Chen, M. J. Park, P. Fragouli and H. Iatrou, *Macromolecules*, 2007, **40**, 4578–4585.
86 J.-l. Shi, H. Li, L.-f. Fang and Z.-y. Liang, *Chin. J. Polym. Sci.*, 2013, **31**, 309–317.
87 C. Monroe and J. Newman, *J. Electrochem. Soc.*, 2005, **152**, A396–A404.
88 Y. Kang, K. Cheong, K. Noh, C. Lee and D. Y. Seung, *J. Power Sources*, 2003, **119–121**, 432–437.
89 T. Tatsuma, M. Taguchi and N. Oyama, *Electrochim. Acta*, 2001, **46**, 1201–1205.
90 X. W. Zhang, Y. Li, S. A. Khan and P. S. Fedkiw, *J. Electrochem. Soc.*, 2004, **151**, A1257–A1263.
91 A. Panday, S. Mullin, E. D. Gomez, N. Wanakule, V. L. Chen, A. Hexemer, J. Pople and N. P. Balsara, *Macromolecules*, 2009, **42**, 4632–4637.
92 E. D. Gomez, A. Panday, E. H. Feng, V. Chen, G. M. Stone, A. M. Minor, C. Kisielowski, K. H. Downing, O. Borodin and G. D. Smith, *Nano Lett.*, 2009, **9**, 1212–1216.
93 K. Kishimoto, M. Yoshio, T. Mukai, M. Yoshizawa, H. Ohno and T. Kato, *J. Am. Chem. Soc.*, 2003, **125**, 3196–3197.
94 N. Rehman, A. Khan, I. Bibi and M. Siddiq, *Chin. J. Polym. Sci.*, 2012, **30**, 217–226.
95 M. B. Armand, *Annu. Rev. Mater. Sci.*, 1986, **16**, 245–261.
96 W. H. Meyer, *Adv. Mater.*, 1998, **10**, 439–448.
97 J. S. Newman and K. E. Thomas-Alyea, *Electrochemical systems*, Wiley, Hoboken, NJ, 2004.
98 O. Borodin and G. D. Smith, *Macromolecules*, 1998, **31**, 8396–8406.
99 O. Borodin and G. D. Smith, *J. Phys. Chem. B*, 2006, **110**, 11481–11490.
100 M. J. Marsella, R. J. Newland, P. J. Carroll and T. M. Swager, *J. Am. Chem. Soc.*, 1995, **117**, 9842–9848.
101 B. C. H. Steele and A. Heinzel, *Nature*, 2001, **414**, 345–352.
102 K. D. Kreuer, S. J. Paddison, E. Spohr and M. Schuster, *Chem. Rev.*, 2004, **104**, 4637–4678.
103 A. E. Javier, S. N. Patel, D. T. Hallinan Jr, V. Srinivasan and N. P. Balsara, *Angew. Chem., Int. Ed.*, 2011, **50**, 9848–9851.
104 M. Armand, F. Endres, D. R. MacFarlane, H. Ohno and B. Scrosati, *Nat. Mater.*, 2009, **8**, 621–629.
105 T. Feng, F. Wu, C. Wu, X. Wang, G. Feng and H. Yang, *Solid State Ionics*, 2012, **221**, 28–34.
106 I. Choi, H. Ahn and M. J. Park, *Macromolecules*, 2011, **44**, 7327–7334.
107 M. J. Park, I. Choi, J. Hong and O. Kim, *J. Appl. Polym. Sci.*, 2013, **129**, 2363–2376.

